AAS 19-285

ROBUST OPTIMISATION OF LOW-THRUST INTERPLANETARY TRANSFERS USING EVIDENCE THEORY

Marilena Di Carlo[*], Massimiliano Vasile[†], C. Greco[‡] and R. Epenoy[§]

This work presents the formulation and solution of optimal control problems under epistemic uncertainty, when this uncertainty is modelled with Dempster-Shaffer theory of evidence. The application is to the design of low-thrust interplanetary transfers when an epistemic uncertainty exists in the performance of the propulsion system and in the magnitude of the departure hyperbolic excess velocity. The problem is solved by transforming the exact formulation, that uses discontinuous Belief functions, into an inexact formulation that uses a new continuous statistical function, called S in the following, that approximates the value of the Belief function. The optimisation is realised by first building a surrogate model of the quantities of interest and associated S functions. The surrogate is then progressively updated as the optimisation proceeds. The proposed method is applied to the design of optimal low-thrust transfers from the Earth to asteroid Apophis.

INTRODUCTION

In the early phases of the design of a space mission, the values of several design parameters are either unknown or are known with a degree of uncertainty.[1] An insufficient consideration for uncertainty, in this phase, would lead to a wrong decision on the feasibility of the mission.[2] In this work, uncertainty quantification is applied to the optimisation of low-thrust interplanetary trajectories. In particular, the optimisation under uncertainty is realised making use of the Dempster-Shaffer theory of evidence,[3] for the case when epistemic uncertainty exists in the system parameters of the low-thrust spacecraft (thrust and specific impulse of the engine) and in the magnitude of the departure hyperbolic excess velocity. The considered problem is a low-thrust transfer from Earth to asteroid Apophis.

The paper is organised as follow. The first two sections introduce the theoretical background required for the formulation of the problem of optimisation under uncertainty. In particular, at first, Uncertainty Quantification using Evidence Theory is presented; then, the Low-Thrust Transfer Optimal Control Problem is described. The problem of Optimisation under Uncertainty is then introduced. The case study and the results of the proposed method are then presented for the Earth-Apophis transfer.

UNCERTAINTY QUANTIFICATION USING EVIDENCE THEORY

Evidence Theory, or Dempster-Shaffer theory, belongs to the class of imprecise probability theories developed to treat both epistemic and aleatory uncertainty, when no information about the probability distribution is available.[4] In Evidence Theory, uncertainties are defined by means of Basic Probability Assignments (BPA), associated to elementary propositions A in the space of possible events Θ. Being Θ the set of all

[*]Research Associate, Department of Mechanical and Aerospace Engineering, University of Strathclyde, 75 Montrose Street, G1 1XJ, Glasgow, United Kingdom.

[†]Professor, Department of Mechanical and Aerospace Engineering, University of Strathclyde, 75 Montrose Street, G1 1XJ, Glasgow, United Kingdom

[‡]PhD Student, Department of Mechanical and Aerospace Engineering, University of Strathclyde, 75 Montrose Street, G1 1XJ, Glasgow, United Kingdom

[§]Engineer, CNES, 18 avenue Edouard Belin 31401 Toulouse Cedex 9, France

possibilities, the Basic Probability Assignment is a function $BPA : 2^{\Theta} \rightarrow [0, 1]$ verifying

$$\begin{aligned} BPA(\emptyset) &= 0\,, \\ \sum_{A \subset \Theta} BPA(A) &= 1\,. \end{aligned} \tag{1}$$

In model-based systems engineering, elementary propositions will often take the form of an uncertain quantity ξ being within a set of intervals, i.e.

$$A = \{\xi \in [a_l, b_l]\}\,, \quad 1 \leq l \leq \mathcal{L}\,, \tag{2}$$

and their associated BPA. In Equation (2), $\mathcal{L}$ is the number of intervals $[a_l, b_l]$ associated to the quantity ξ. Note that BPA can be associated to potentially overlapping or disjoint intervals as well as to their union, the latter representing a degree of ignorance. If several uncertain variables are taken into account, one will consider propositions of the kind

$$A = \{\boldsymbol{\xi} = (\xi_1, \xi_2, \cdots, \xi_{n_\xi}) \in \prod_{j=1}^{n_\xi} [a_{j,l_j}, b_{j,l_j}] = H_{\mathbf{l}}\}\,, \quad 1 \leq l_j \leq \mathcal{L}_j\,, \tag{3}$$

where n_ξ is the number of uncertain variables and $[a_{j,l_j}, b_{j,l_j}]$ denote the bounds of the l_j-th interval of the j-th variables. In Equation (3), $\mathbf{l} = (l_1, l_2, \cdots, l_{n_\xi})$ is the multivariate index associated to hyperrectangular domain $H_{\mathbf{l}}$. Assuming independent uncertainties, the BPA of every such possibility can be computed as the product of the BPA of the elementary propositions regarding each ξ_j,

$$BPA(H_{\mathbf{l}}) = \prod_{j=1}^{n_\xi} BPA_{j,l_j}\,, \tag{4}$$

where BPA_{j,l_j} is the BPA associated to the interval l_j of the uncertain variable j. After combination of several, possibly conflicting, evidence sources,[5–7] a map of probability masses is thus assigned to all elements in 2^{Θ}. The Belief (Bel) on and Plausibility (Pl) of a given proposition $A \subseteq \Theta$ are defined as

$$\begin{aligned} Bel(A) &= \sum_{B|B \subseteq A} BPA(B)\,, \\ Pl(A) &= \sum_{B|B \cap A \neq \emptyset} BPA(B)\,, \end{aligned} \tag{5}$$

i.e. $Bel(A)$ collects the BPA associated to possibilities B satisfying A, whereas $Pl(A)$ collects the BPA of possibilities B not contradicting A. Hence

$$Pl(A) = 1 - Bel(\bar{A})\,, \tag{6}$$

and Belief and Plausibility can be interpreted as the lower and upper bounds, respectively, imposed by the evidence available on the imprecise probability $P(A)$. The difference between $Pl(A)$ and $Bel(A)$ constitutes an indicator of the degree of second-order uncertainty associated to the assessment of $P(A)$. This interpretation is illustrated in Figure 1.

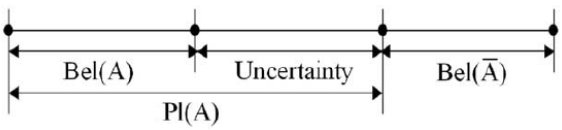

Figure 1: Interpretation of the relation between Belief, Plausibility and (second-order) uncertainty on $P(A)$.

In the applications that concern this work, the formulation presented translates into considering a mapping of BPA over a family of hyperrectangular subsets H_1 of the space of uncertain variables. This family of subsets is referred to as Ξ, the uncertainty space, and needs to contain every focal element θ, that is every subset of Θ with non-null BPA:

$$\Xi \supseteq \bigcup \theta \,,\ \theta \subset \Theta \,,\ BPA(\theta) > 0 \,. \tag{7}$$

The BPA structure of Ξ can then be used to calculate the lower (Belief) and upper (Plausibility) bounds on the probability that the value of a quantity of interest $J(\boldsymbol{\xi})$ is as expected, e.g. under a threshold ν, by considering

$$A = \{\boldsymbol{\xi} \in \Xi \,|\, J(\boldsymbol{\xi}) \leq \nu\} \,, \tag{8}$$

which gives

$$\begin{aligned} Bel(J(\boldsymbol{\xi}) \leq \nu) &= \sum_{\overline{\theta}} BPA(\theta) \,, \\ Pl(J(\boldsymbol{\xi}) \leq \nu) &= \sum_{\underline{\theta}} BPA(\theta) \,, \end{aligned} \tag{9}$$

with

$$\begin{aligned} \overline{\theta} &= \{\theta \subset \Theta | \max_{\boldsymbol{\xi} \in H_1 \subseteq \theta} (J(\boldsymbol{\xi})) \leq \nu \}, \\ \underline{\theta} &= \{\theta \subset \Theta | \min_{\boldsymbol{\xi} \in H_1 \subseteq \theta} (F(\boldsymbol{\xi})) \leq \nu \}. \end{aligned} \tag{10}$$

Thus, in robust design optimisation, the robustness of a design against the epistemic uncertainty in the system is usually characterised by the curves $Bel(J(\boldsymbol{\xi}) \leq \nu)$ and $Pl(J(\boldsymbol{\xi}) \leq \nu)$ against ν associated to that design – henceforth referred to simply as Belief and Plausibility curves. In particular, if J is to be minimised, then A as defined above is the desirable hypothesis, and the robustness index is often chosen as $Bel(J(\boldsymbol{\xi}) \leq \nu)$ since it can be interpreted as a conservative estimation of the probability associated to the desirable hypothesis. The drawback of this comprehensive approach for uncertainty quantification is that it leads to an NP-hard problem with a computational complexity that is exponential with the number of epistemic uncertain variables. This is due to the fact that a global maximisation (or minimisation) of the quantity of interest is required over each $\theta \subset \Xi$ having non-null BPA (Equation (10)). In this work this issue is tackled using surrogate models of the quantities of interest, in order to reduce the computational time associated to the minimisation and maximisation. The single objective optimisation problems given in Equations (10) are solved using Multi-Population Adaptive Inflationary Differential Evolution Algorithm (MP-AIDEA),[8] an adaptive multi-population evolutionary algorithm based on the hybridisation of Differential Evolution with Monotonic Basin Hopping. MP-AIDEA is available open-source on GitHub at `https://github.com/strath-ace/smart-o2c/tree/master/Optimisation`.

LOW-THRUST TRANSFER OPTIMAL CONTROL PROBLEM

The use of Evidence Theory to treat uncertainties is applied to the optimal control problem of an interplanetary low-thrust transfer. The low-thrust optimal control problem is transcribed with a variant of the direct analytical shooting algorithm proposed by Zuiani et al.[9] and implemented in the software code FABLE (FAst Boundary-value Low-thrust Estimator).[10] The code FABLE is available open source on GitHub at `https://github.com/strath-ace/smart-o2c/tree/development/Transcription/FABLE`. The idea of this transcription method is to split the trajectory into a predefined sequence of n_{LT} finite coast and thrust arcs. Each s-th thrust arc is represented by the low-thrust acceleration components, a_r, a_t and a_h expressed in a local radial-transverse-normal reference frame as:[9]

$$\mathbf{a}_{LT,s} = \begin{Bmatrix} a_r \\ a_t \\ a_h \end{Bmatrix}_s = \begin{Bmatrix} \epsilon_s \cos\alpha_s \cos\beta_s \\ \epsilon_s \sin\alpha_s \cos\beta_s \\ \epsilon_s \sin\beta_s \end{Bmatrix} \,, \tag{11}$$

where α_s and β_s are, respectively, the azimuth and elevation angles and ϵ_s is the modulus of the acceleration:

$$\epsilon_s = \frac{F}{m_s} \frac{1}{(r/\bar{r})^2} \ . \tag{12}$$

In Equation (12), F is the thrust of the engine, m_s is the mass of the spacecraft on the s-th arc, and $\bar{r} = 1$ AU. The trajectory is analytically propagated from the departure point to the arrival point. The departure state is defined by the state of the Earth on the departure day; the departure velocity vector is obtained considering both the velocity of the Earth and the departure hyperbolic excess velocity vector $\mathbf{v}_\infty$, defined, in an Earth-centered reference system, as:

$$\mathbf{v}_\infty = [v_\infty \cos\alpha \cos\delta, v_\infty \sin\alpha \cos\delta, v_\infty \sin\delta]^T \ . \tag{13}$$

In Equation (13), α and δ are the departure azimuth and declination angles. The arrival state is defined by the state of the target body on the arrival day, considering a two-body dynamics. The motion of the spacecraft is assumed purely Keplerian along coast arcs while thrust arcs are analytically propagated using an asymptotic expansion solution based on the work of Zuiani and Vasile.[11] Each arc begins and ends at an On/Off control node, where On nodes define the switching point from a coast to a thrust arc and Off nodes define the switching point from a thrust to a coast arc. The azimuth and elevation angles, α_s and β_s, are constant along a thrust arc, while ϵ_s changes according to Equation (12). The optimisable vector for each transfer is defined by the angles α_s and β_s for each thrust arc, by the true longitude of the On/Off control nodes, and by the azimuth and declination angles at lunch (the magnitude v_∞ is assumed to be known):

$$\mathbf{u} = [L_{1,On}, L_{1,Off}, \alpha_1, \beta_1, L_{2,On}, L_{2,Off}, \alpha_2, \beta_2, \ldots L_{n_{LT},On}, L_{n_{LT},Off}, \alpha_{n_{LT}}, \beta_{n_{LT}}, \alpha, \delta]^T \ . \tag{14}$$

The objective function of the optimal control problem is the total ΔV, calculated as:

$$J(\mathbf{u}, v_\infty, F, I_{sp}) = \Delta V = \sum_{s=1}^{n_{LT}} \int \epsilon_s \, dt = \int \frac{F \, \bar{r}^2}{r(t)^2 \, m(t)} dt \ . \tag{15}$$

In the conservative assumption that m stays constant on each thrust arc, the integrals for the computation of ΔV can be transformed into integrals in the true longitude L, that can be solved analytically to give:

$$J(\mathbf{u}, v_\infty, F, I_{sp}) = \Delta V \approx \sum_{s=1}^{n_{LT}} \frac{F \, \bar{r}^2}{m_s} \frac{1}{\sqrt{\mu a_s (1 - e_s^2)}} \Delta L_s \ , \tag{16}$$

where a_s, e_s and m_s are, respectively, the semi-major axis, eccentricity and mass at the beginning of the s-th thrust arc, and $\Delta L_s = L_{s,Off} - L_{s,On}$ is the variation of the true longitude on the thrust arc. The values of a_s and e_s, for $s = 1$, depend upon v_∞; the mass m_s is updated at the end of each thrust arc using the considered value of the specific impulse, according to:

$$m_{s+1} = m_s - \frac{F}{\sqrt{\mu a_s (1 - e_s^2)}} \frac{\Delta L_s}{I_{sp} g_0} \ . \tag{17}$$

The analytical expression in Equation (16) is obtained from Equation (15) using:[9]

$$\frac{dt}{dL} = \sqrt{\frac{a^3}{\mu}} \frac{(1 - e^2)^3}{(1 + P_1 \sin L + P_2 \cos L)^2} \tag{18}$$

and

$$r(L) = \frac{a \, (1 - e^2)}{(1 + P_1 \sin L + P_2 \cos L)} \ , \tag{19}$$

where $P_1 = 1 + e \sin(\Omega + \omega)$ and $P_2 = 1 + e \cos(\Omega + \omega)$ are the second and third equinoctial elements, Ω is the right ascension of the ascending node and ω is the argument of the periapsis. Note that Equation

(18) is an approximated expression that does not include the direct effect of the thrust on the variation of L. This approximation provides acceptable results for control acceleration levels that are typical of existing low-thrust propulsion systems. The use of the analytical expression for J speeds up the optimisation process with respect to the use of a numerical integration, while still giving accurate results. The non-linear programming problem to solve is:

$$\begin{aligned} &\min_{\mathbf{u}\in U} J(\mathbf{u}, v_\infty, F, I_{sp}) \\ &\text{s.t.} \quad \mathbf{x}_{final} = \bar{\mathbf{x}}_f \\ &\qquad \sum_{s=1}^{n_{LT}} \Delta t_s = ToF \end{aligned} \tag{20}$$

where $\mathbf{x}_{final}$ is the final state of the spacecraft at the end of the propagation, $\bar{\mathbf{x}}_f$ is the desired arrival state and ToF is the desired time of flight. The non-linear programming problem is solved using the Matlab® *fmincon-interior-point* algorithm.

OPTIMISATION UNDER UNCERTAINTY

The previous two sections have presented the formulation of the uncertainty quantification using Evidence Theory and the formulation of the low-thrust transfer optimal control problem. These two concepts will be now combined to define the problem of optimisation under uncertainty of a low-thrust transfer, using Evidence Theory. The problem is formulated as follows:

$$\begin{aligned} &\max_{\mathbf{u}\in U} Bel(J(\mathbf{x}, \mathbf{u}, \boldsymbol{\xi}) \in \Psi) \\ &\text{s.t.} \quad \dot{\mathbf{x}} = \mathbf{f}(\mathbf{x}, \mathbf{u}, \boldsymbol{\xi}, t) \\ &\qquad \mathbf{g}(\mathbf{x}, \mathbf{u}, \boldsymbol{\xi}, t) \geq 0 \\ &\qquad Bel\left(\boldsymbol{\psi}\left(\mathbf{x}_0, \mathbf{x}_f(\boldsymbol{\xi}), t_0, t_f\right) \in \Phi\right) > 1 - \varepsilon \\ &\qquad t \in [t_0, t_f] \end{aligned} \tag{21}$$

where $\mathbf{x} \in \mathcal{R}^n$ is the state vector, $\mathbf{u}$ the control vector, $\boldsymbol{\xi}$ the uncertainty vector of dimension n_ξ, t the time, $\boldsymbol{f}$ the dynamic of the system, $\boldsymbol{\psi}$ the function defining the final state of the system and Φ the target set. The subscripts 0 and f denote initial and final conditions, respectively. The goal is to maximize the belief Bel, or lower probability, that the cost function J belongs to the set Ψ, with the belief Bel of constraint satisfaction being greater than a given positive value $1 - \varepsilon$.

In the following, Problem (22) will be specifically written and expressed for the case of a low-thrust transfer. In this case, the optimal control problem under uncertainty is formulated as:

$$\begin{aligned} &\max_{\mathbf{u}\in U} Bel(m_{prop} \leq \bar{\nu}_{m_{prop}}) \\ &\text{s.t.} \quad \dot{\mathbf{x}} = \mathbf{f}(\mathbf{x}, \mathbf{u}, \boldsymbol{\xi}, t) \\ &\qquad Bel\left(\Delta r \leq \bar{\nu}_{\Delta r}\right) > 1 - \varepsilon_{\Delta r} \\ &\qquad Bel\left(\Delta v \leq \bar{\nu}_{\Delta v}\right) > 1 - \varepsilon_{\Delta v} \end{aligned} \tag{22}$$

The goal is to find the control $\mathbf{u}$, in the space of the controls U, that maximise the belief Bel that the mass of propellant m_{prop} is lower or equal than a threshold $\bar{\nu}_{m_{prop}}$. At the same time, the control must satisfy some position and velocity constraints expressed in terms of the Belief function. In particular, given the thresholds $\bar{\nu}_{\Delta r}$ and $\bar{\nu}_{\Delta v}$ for the position and the velocity constraint violations Δr and Δv, it is required for the Belief of $\Delta r \leq \bar{\nu}_{\Delta r}$ and the Belief of $\Delta v \leq \bar{\nu}_{\Delta v}$ to be greater than $1 - \epsilon_{\Delta r}$ and $1 - \epsilon_{\Delta v}$, respectively.

The solution of Problem (22) presents some difficulties, from a computational point of view. In particular:

- the computation of the Belief function for each control $\mathbf{u}$ requires the solution of a maximisation problem,[2] over all the focal elements of the uncertainty space;
- the optimisation of the function Bel has to be realised over the control domain U, that is a high-dimensional space.

- the function Bel is discontinuous and cannot be easily represented with a surrogate model. On the other hand, the availability of a surrogate for Bel would avoid the need to realise the maximisation of the quantities of interest over all the focal elements, and for each new control vector (a procedure that is required to compute the Belief).

In this paper, these challenges are addressed with a combination of the following techniques:

- surrogate models of the quantities of interest, m_{prop}, Δr and Δv, are used to speed up the maximisation over each focal element, for each control vector $\mathbf{u}$; these surrogate models will be called "internal" in the following, and will be denoted with the symbols $\tilde{m}_{prop}$, $\widetilde{\Delta r}$ and $\widetilde{\Delta v}$;
- given that the uncertainty space Ξ is smaller than the control space U, a dimensionality reduction method is devised so that Problem (22) can be solved over the space of the uncertain parameters Ξ, rather than the space of the controls U;
- surrogate models are used to represent a continuous approximation of the Bel function, so that the optimisation of Problem (22) can be realised on a continuous surrogate model of the continuous approximation of Bel. The continuous approximation of Bel will be called S in the following, and its surrogate $\tilde{S}$ will be called "external" surrogate.

By using these three techniques, Problem (22) can be formulated as:

$$\begin{aligned} &\max_{\boldsymbol{\xi}\in\Xi} \tilde{S}(\tilde{m}_{prop} \leq \bar{\nu}_{m_{prop}}) \\ &\text{s.t.} \quad \tilde{S}\left(\widetilde{\Delta r} \leq \bar{\nu}_{\Delta r}\right) > 1 - \varepsilon_{\Delta r,S} \\ &\qquad \tilde{S}\left(\widetilde{\Delta v} \leq \bar{\nu}_{\Delta v}\right) > 1 - \varepsilon_{\Delta v,S} \end{aligned} \tag{23}$$

The variables $\varepsilon_{\Delta r,S}$ and $\varepsilon_{\Delta r,S}$ in Problem 23 are related to the variables $\varepsilon_{\Delta r}$ and $\varepsilon_{\Delta r}$ of Problem (22). A detailed explanation of the relationship between $\varepsilon_{\Delta r,S}$ and $\varepsilon_{\Delta r,S}$ and $\varepsilon_{\Delta r}$ and $\varepsilon_{\Delta r}$ willl be given in the following. The next subsections will give more details about the correspondence between Ξ and U, the internal and external surrogate models, and the function S.

Dimensionality Reduction and Mapping Between Ξ and U

In this work it is assumed that for a given uncertain vector $\bar{\boldsymbol{\xi}}$ there is one and only one control $\bar{\mathbf{u}}$ that is globally optimising the quantity of interest and satisfying the constraints. This implies that we can define a one-to-one functional relationship between the space of the feasible and global optima controls U and the space of the uncertain parameters Ξ. This one-to-one correspondence can be used to replace the optimisation vector $\mathbf{u}$ with the smaller dimensional optimisation vector $\boldsymbol{\xi}$. The functional relationship can be recovered through the solution of Problem (20). In fact, for a given value of $\bar{\boldsymbol{\xi}}$, and using Equations (33) to (35), $\bar{\boldsymbol{\xi}}$ will be uniquely associated to a vector of controls $\bar{\mathbf{u}}$. The criticality of this dimensionality reduction approach is the identification of the feasible and global optimal control law. Although this identification is theoretically possible, it is also practically challenging. On the other hand, one can accept also the identification of a local minimum, as long as local minima are unique, because local minima correspond to conservative solution of the proposition $(m_{prop} \leq \bar{\nu}_{m_{prop}})$, for which the Bel needs to be maximised. While in this paper the analysis is restricted to the space of the feasible and optimal controls, future work will be devoted to extend the study to the space of all the control laws, including the non feasible and non optimal ones.

Internal Surrogate Models

Internal surrogate models are used to model the functions $m_{prop}(\boldsymbol{\xi}, \bar{\mathbf{u}})$, $\Delta r(\boldsymbol{\xi}, \bar{\mathbf{u}})$ and $\Delta v(\boldsymbol{\xi}, \bar{\mathbf{u}})$. These functions express the value of the mass of propellant and position and velocity constraints associated to a given control solution $\bar{\mathbf{u}}$, when the uncertain vector has values different from the ones associated to $\bar{\mathbf{u}}$, that is when $\boldsymbol{\xi} \neq \bar{\boldsymbol{\xi}}$. More in details, the three internal surrogate models are:

1. A surrogate model for the propellant mass, for different values of the uncertainty vector $\boldsymbol{\xi}$, and for a fixed value of the control vector $\bar{\mathbf{u}}$:

$$\tilde{m}_{prop}\left(\boldsymbol{\xi}, \bar{\mathbf{u}}\right) \approx m_{prop}\left(\boldsymbol{\xi}, \bar{\mathbf{u}}\right) \quad \boldsymbol{\xi} \in \Xi \tag{24}$$

   The surrogate model $\tilde{m}_{prop}$ describes how the mass of propellant required to realise the transfer changes when the system parameters are different from $\bar{\boldsymbol{\xi}}$, but the control is kept equal to $\bar{\mathbf{u}}$.

2. A surrogate model for the violation of the final constraints on the position:

$$\widetilde{\Delta r}\left(\boldsymbol{\xi}, \bar{\mathbf{u}}\right) \approx \Delta r\left(\boldsymbol{\xi}, \bar{\mathbf{u}}\right) \quad \boldsymbol{\xi} \in \Xi \tag{25}$$

   The surrogate model $\widetilde{\Delta r}$ describes how the final violation of the constraint on the position changes when the system parameters are different from $\bar{\boldsymbol{\xi}}$, but the control is kept equal to the control $\bar{\mathbf{u}}$.

3. A surrogate model for the violation of the final constraints on the velocity:

$$\widetilde{\Delta v}\left(\boldsymbol{\xi}, \bar{\mathbf{u}}\right) \approx \Delta v\left(\boldsymbol{\xi}, \bar{\mathbf{u}}\right) \quad \boldsymbol{\xi} \in \Xi \tag{26}$$

The responses of the training points used to build the surrogate models, $\mathcal{T} = \left\{\boldsymbol{\xi}_p\right\}_{p=1}^{N_p}$, are obtained propagating the dynamic equations for the motion of the spacecraft using the nominal control $\bar{\mathbf{u}}$ and different values of the uncertainty vector $\boldsymbol{\xi}$. For a given control $\bar{\mathbf{u}}$ and set of uncertain parameters $\boldsymbol{\xi}$, the state vector $\mathbf{x} = \left[\mathbf{r}, \mathbf{v}, m\right]^T$ of the spacecraft at time t_f is computed as:

$$\mathbf{x}\left(\boldsymbol{\xi}, \bar{\mathbf{u}}, t_f\right) = \left[\mathbf{r}\left(\boldsymbol{\xi}, \bar{\mathbf{u}}, t_f\right), \mathbf{v}\left(\boldsymbol{\xi}, \bar{\mathbf{u}}, t_f\right), m\left(\boldsymbol{\xi}, \bar{\boldsymbol{u}}, t_f\right)\right]^T = \mathbf{x}_0 + \int_{t_0}^{t_f} \mathbf{f}\left(\mathbf{x}, \bar{\mathbf{u}}, \boldsymbol{\xi}, t\right) dt \, . \tag{27}$$

The integration in Equation (27) is performed analytically, using a first order expansion in the perturbing acceleration.[11] The responses of the training points for the three surrogate models are computed as:

$$\begin{aligned} m_{prop} &= m_0 - m\left(\boldsymbol{\xi}, \bar{\boldsymbol{u}}, t_f\right) \\ \Delta r &= \left\|\mathbf{r}\left(\boldsymbol{\xi}, \bar{\mathbf{u}}, t_f\right) - \mathbf{r}_{target}\right\| \\ \Delta v &= \left\|\mathbf{v}\left(\boldsymbol{\xi}, \bar{\mathbf{u}}, t_f\right) - \mathbf{v}_{target}\right\| \, , \end{aligned} \tag{28}$$

where m_0 is the initial mass of the spacecraft at launch, and $\mathbf{r}_{target}$ and $\mathbf{v}_{target}$ are the targeted position and velocity vectors. The use of the surrogate models replace, therefore, the propagation in Equation (27) with the evaluation of the surrogate functions. The surrogate models are generated from the training points $\mathcal{T}$, and the corresponding m_{prop}, Δr and Δv computed through Equation (28), using the Matlab toolbox DACE.[12]

The Smooth Bel/Pl Function

The use of the internal surrogate models speeds up the computation of the Belief. This makes the computation of the Belief associated to a single uncertain vector $\bar{\boldsymbol{\xi}}$ and corresponding control $\bar{\mathbf{u}}$ relatively fast, but the computation is still not fast enough for the evaluations of the function at several points, as required by the solution of Problem (22). The solution of Problems (22) requires, in fact, an optimisation process that has to evaluate the Bel at several points $\boldsymbol{\xi}$. To solve this difficulty, surrogate models of the functions $Bel(m_{prop} \leq \bar{\nu}_{m_{prop}})$, $Bel(\Delta r \leq \bar{\nu}_{\Delta r})$ and $Bel(\Delta v \leq \bar{\nu}_{\Delta v})$ could be built, so as to speed up the optimisation. These surrogate models are denoted as "external". However, the Belief is a discontinuous function, and it is difficult to create the surrogate model of a discontinuous function. To avoid the problems associated with the creation of the surrogate model of the Belief, and with the optimisation of a discontinuous function, the Belief is substituted by a continuous function. The external surrogate models are then built for the continuous function that substitutes the Belief, rather than for the Belief itself. The continuous function that substitutes the Belief, denoted as S, is referred to as "Smooth Bel/Pl function". The function S is defined as:

$$S\left(J\left(\boldsymbol{\xi}\right) \leq \nu\right) = \sum_{\theta \in \Theta} BPA\left(\theta\right) \left[\frac{\int_{\theta} \mathbb{1}\left(J\left(\boldsymbol{\xi}\right) \leq \nu\right) d\boldsymbol{\xi}}{V_\theta}\right]^k \, , \tag{29}$$

where V_θ is the hypervolume of the focal element θ and $\mathbb{1}$ is the indicator function. Due to the normalisation of the integral at the numerator of Equation 29 with V_θ, the term in square brackets will assume only values in the range $[0, 1]$. The integral in Equation (29) is computed by sampling each focal element θ at a given number of points, and then numerically integrating, via Monte Carlo integration, a function that assumes values equal to 1 at the sampling points where the inequalities are satisfied, and 0 at the sampling points where the inequalities are not satisfied. Figure 2 shows a graphical representation of the computation of the integral in the function S, for a one-dimensional example with two focal elements, FE_1 and FE_2, characterised by BPA_1 and BPA_2. In particular, with reference to Figure 2:

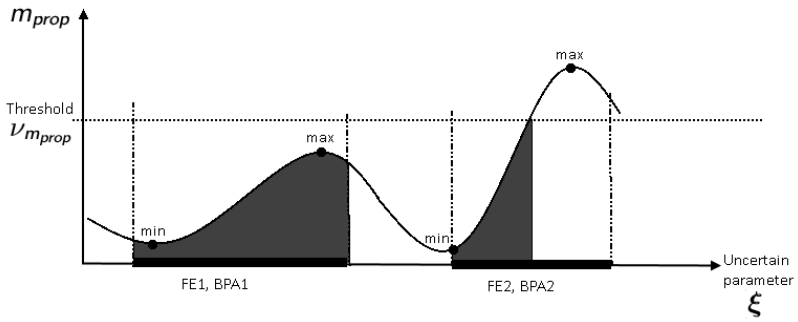

Figure 2: Graphical representation for the computation of the integral in Equation (29).

$$\begin{aligned} Bel &= BPA_1 \\ Pl &= BPA_1 + BPA_2 \\ S &= BPA_1 \cdot 1^k + BPA_2 \cdot 0.5^k \end{aligned} \tag{30}$$

and therefore

$$Bel \leq S \leq Pl\ . \tag{31}$$

The function S coincides with Bel and Pl when $k \to \infty$ and $k = 0$, respectively. The Belief, Plausibility and function S, for different values of k, are represented in Figure 3 for a given control $\hat{\mathbf{u}}$. Figure 3 shows that S is always $Bel \leq S \leq Pl$.

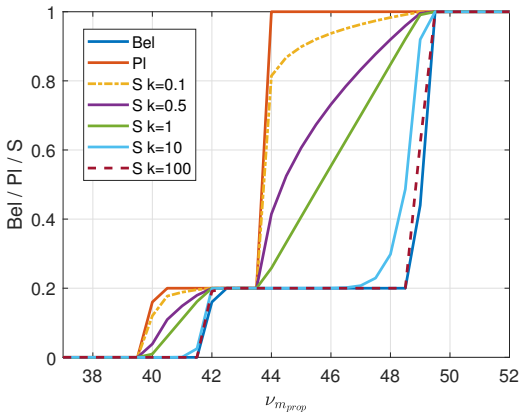

Figure 3: Bel, Pl and S curves for the mass of propellant.

In the new formulation of Problem (22), introduced in Equation (23), the objective function $Bel(m_{prop} \leq \bar{\nu}_{m_{prop}})$ is substituted by the surrogate of $S_{m_{prop}} = S(m_{prop} \leq \bar{\nu}_{m_{prop}})$, denoted as $\widetilde{S}_{m_{prop}}$. Analogously,

$Bel(\Delta r \leq \bar{\nu}_{\Delta r})$ and $Bel(\Delta v \leq \bar{\nu}_{\Delta r})$ are substituted by $\widetilde{S}_{\Delta r} \approx S_{\Delta r} = S(\Delta r \leq \bar{\nu}_{\Delta r})$ and $\widetilde{S}_{\Delta v} \approx S_{\Delta v} = S(\Delta v \leq \bar{\nu}_{\Delta v})$, respectively. Finally, by performing the optimisation in the space Ξ rather than U, Problem (22) becomes:

$$\begin{aligned} &\max_{\boldsymbol{\xi} \in \Xi} \widetilde{S}_{m_{prop}} \\ &\text{s.t.} \quad \widetilde{S}_{\Delta r} > 1 - \varepsilon_{\Delta r,S} \\ &\qquad \widetilde{S}_{\Delta v} > 1 - \varepsilon_{\Delta v,S} \end{aligned} \tag{32}$$

which is equivalent to Problem (23). In Problem (32), the quantities $\varepsilon_{\Delta r,S}$ and $\varepsilon_{\Delta v,S}$ must satisfy $\varepsilon_{\Delta r,S} \leq \varepsilon_{\Delta r}$ and $\varepsilon_{\Delta v,S} \leq \varepsilon_{\Delta v}$, where $\varepsilon_{\Delta r}$ and $\varepsilon_{\Delta v}$ have been defined in Problem (22). The values of $\epsilon_{\Delta r,S}$ and $\epsilon_{\Delta v,S}$ are obtained from an iterative process that starts from $\epsilon^0_{\Delta r,S} = \epsilon_{\Delta r}$ and $\epsilon^0_{\Delta v,S} = \epsilon_{\Delta v}$ and proceed by decreasing $\epsilon_{\Delta r,S}$ and $\epsilon_{\Delta v,S}$ at each step. This iteration process is necessary because of the property of function S of being always $S \geq Bel$ (Figure 3); as a consequence, a point $\boldsymbol{\xi}$ satisfying $Bel_{\Delta r} > 1 - \epsilon_{\Delta r}$ and $Bel_{\Delta_v} > 1 - \epsilon_{\Delta v}$ might not satisfy $S_{\Delta r} > 1 - \epsilon_{\Delta r}$ and $S_{\Delta_v} > 1 - \epsilon_{\Delta v}$. The iterations stop when values of $\epsilon_{\Delta r,S}$ and $\epsilon_{\Delta v,s}$ are reached such that when $Bel_{\Delta r} > 1 - \epsilon_{\Delta r}$ also $S_{\Delta r} > 1 - \epsilon_{\Delta r,S}$, and when $Bel_{\Delta v} > 1 - \epsilon_{\Delta v}$ also $S_{\Delta v} > 1 - \epsilon_{\Delta v,S}$.

Summary of the Proposed Solution Method

The diagram flows in Figures 4 and 5 summarise the proposed solution method for the optimal control problem under uncertainty. The first step is the generation of N training points in the uncertaint space Ξ (Figure 4); these are defined using an Halton sequence. Each one of the training points is evaluated using the method described in Figure 5, in order to obtain the corresponding values of the Bel and S functions. The values of these functions, for all the training points, are then collected, and DACE is used to generate the external surrogate models $\tilde{S}$. Using $\tilde{S}$, Problem (32) is solved, making use of the algorithm MP-AIDEA. The optimal uncertain vector $\boldsymbol{\xi}_{opt}$, solution of Problem (32), is evaluated using the method described in Figure 5. The new value of S corresponding to $\boldsymbol{\xi}_{opt}$ is used to update the external surrogate models. The process stops when the maximum number of iterations is reached. The iterative process allows to update the external surrogate models after each optimisation, so that accurate surrogate models can be locally obtained in the region where the solutions of the problem are located. The evaluation of Bel and S for a single point $\boldsymbol{\xi}$ follows the method described in Figure 5. The first step is the solution of the NLP problem corresponding to Problem (20), for the given vector of uncertain parameters $\bar{\boldsymbol{\xi}}$. As already mentioned, the solution of the NLP problem provides a solution vector which uniquely identifies a vector of control $\bar{\mathbf{u}}$. Using $\bar{\mathbf{u}}$, the internal surrogate models can be computed, from which the values of Bel and S can then be obtained.

CASE STUDY: EARTH-APOPHIS LOW-THRUST TRANSFER

The computational framework described in this paper is applied to the design of a simple low-thrust trajectory from the Earth to asteroid Apophis. The considered transfer starts on 22 October 2026. The arrival date at Apophis is 11 July 2028. The orbital elements for the asteroid Apophis, for the epoch 24 September 2008, are taken from the JPL Small-Body Database*. The state of Apophis at the arrival date 11 July 2028, $\bar{\mathbf{x}}_f$, is then computed considering a Keplerian motion around the Sun. The mass of the spacecraft at departure is 644.3 kg. This section will introduce the considered vector of uncertaint parameters, the nominal trajectory, and the results of the optimisation under uncertainty.

Uncertain Parameters

The considered uncertain parameters are the magnitude v_∞ of the departure hyperbolic excess velocity vector, and the values of the thrust F and specific impulse I_{sp} of the engine during the transfer. In particular, it is assumed that the thrust and the specific impulse are subject to an uncertainty that is linearly dependent on the position of the spacecraft along its trajectory (denoted by the true longitude L):

$$F(L) = F_1 + F_2 L, \qquad I_{sp}(L) = I_{sp_1} + I_{sp_2} L \,. \tag{33}$$

*https://ssd.jpl.nasa.gov/sbdb.cgi#top

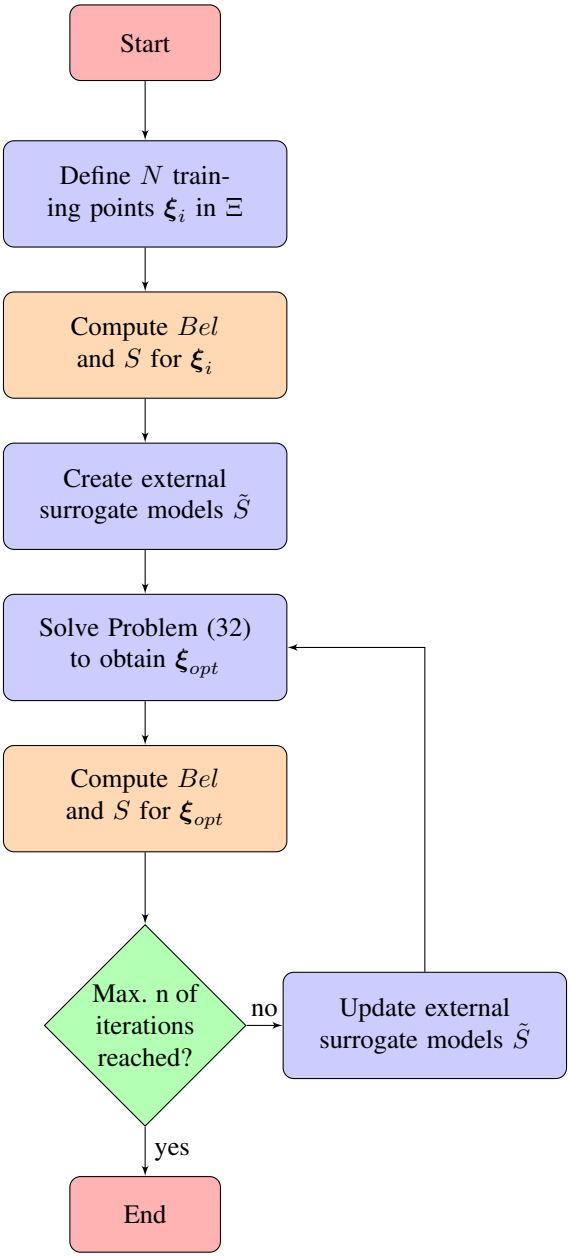

Figure 4: Summary of the proposed solution method for the solution of the optimal control problem under uncertainty.

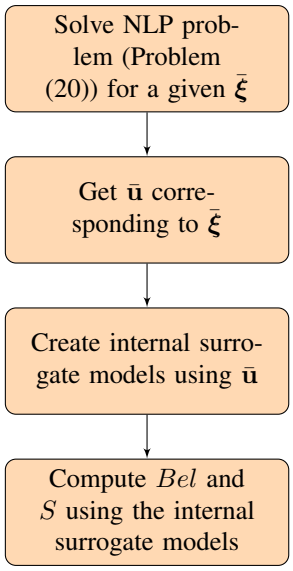

Figure 5: Computation of Bel and S corresponding to a vector $\bar{\boldsymbol{\xi}}$ of uncertain parameters.

The variables F_1, F_2 and I_{sp_1}, I_{sp_2} can be expressed using the values of the thrust and specific impulse at the initial and final true longitudes of the transfer, L_0 and L_f:

$$\begin{aligned} F_{L_0} &= F(L_0) = F_1 + F_2 L_0 \,, \qquad I_{sp,L_0} = I_{sp}(L_0) = I_{sp_1} + I_{sp_2} L_0 \,, \\ F_{L_f} &= F(L_f) = F_1 + F L_f \,, \qquad I_{sp,L_f} = I_{sp}(L_f) = I_{sp_1} + I_{sp_2} L_f \,. \end{aligned} \tag{34}$$

The quantities F_1, F_2, I_{sp_1} and I_{sp_2} can be derived from F_{L_0}, F_{L_f}, I_{sp,L_0} and I_{sp,L_f} using:

$$\begin{aligned} F_1 &= \frac{F_{L_0} L_f - F_{L_f} L_0}{L_f - L_0} \,, \\ \mathrm{F}_2 &= \frac{F_{L_f} - F_{L_0}}{L_f - L_0} \,. \end{aligned} \tag{35}$$

The vector of uncertain variables includes, therefore, five parameters: $\boldsymbol{\xi} = \left[v_\infty, F_{L_0}, F_{L_f}, I_{sp,L_0}, I_{sp,L_f}\right]^T$. The range for the uncertain parameters is reported in Table 1, where $\boldsymbol{\xi}^L$ denotes the lower bound and $\boldsymbol{\xi}^U$ the upper bound.

Table 1: Uncertainty range of the uncertain parameters.

	v_∞ [km/s]	I_{sp,L_0} [s]	I_{sp,L_f} [s]	F_{L_0} [N]	F_{L_f} [N]
$\boldsymbol{\xi}^L$	3	2772	2772	0.0477	0.0477
$\boldsymbol{\xi}^U$	3.7	3388	3388	0.0583	0.0583

Nominal Trajectory

The nominal values of the system parameters are reported in Table 2. The nominal low-thrust optimisation

Table 2: Nominal values of the system parameters.

	v_∞ [km/s]	$I_{sp,L_0}[s]$	I_{sp,L_f} [s]	F_{L_0} [N]	F_{L_f} [N]
Nominal	3.34	3080	3080	0.053	0.053

problem is solved using the solution method described in the Section titled "Low-Thrust Transfer Optimal Control Problem". Figure 6 shows the projection in the x-y plane of the trajectory of the spacecraft and the distance of the spacecraft from the Sun during the transfer; coast arcs are represented in green and thrust arcs in red. Figure 7 shows the variation of semi-major axis and inclination of the spacecraft during the transfer.

The ΔV of the transfer is 2.1584 km/s, corresponding to a propellant mass of 44.95 kg. The optimal declination angle at departure is -12.395 deg. The difference in position between the spacecraft and Apophis at the end of the transfer is 124.17 km; the difference in velocity is 2.3 10^{-5} km/s.

Optimisation Under Uncertainty

The nominal solution presented in the previous section represents an optimal and feasible solution only for the values of the uncertain parameters defined in Table 2. If the nominal control vector is used with a set of uncertain parameters different from those in Table 2 (for example, because v_∞ changes at launch, or because I_{sp} and F change during the transfer), the nominal control could not guarantee that Apophis could be reached. In order to find the control law that is robust against variations of the parameters $\boldsymbol{\xi}$, it is necessary to solve a problem of optimisation under uncertainty.

Problem Definition Since under uncertainty the goal is to attain a target set, the following problem has been considered:

$$\begin{aligned} &\max_{\boldsymbol{\xi} \in \Xi} \; Bel\left(m_{prop} \leq 47 \text{ kg}\right) \\ &\text{s.t.} \quad Bel(\Delta r \leq 3.2\ 10^6 \text{ km}) > 0.95 \\ &\qquad\; Bel(\Delta v \leq 0.91 \text{ km/s}) > 0.95 \,. \end{aligned} \tag{36}$$

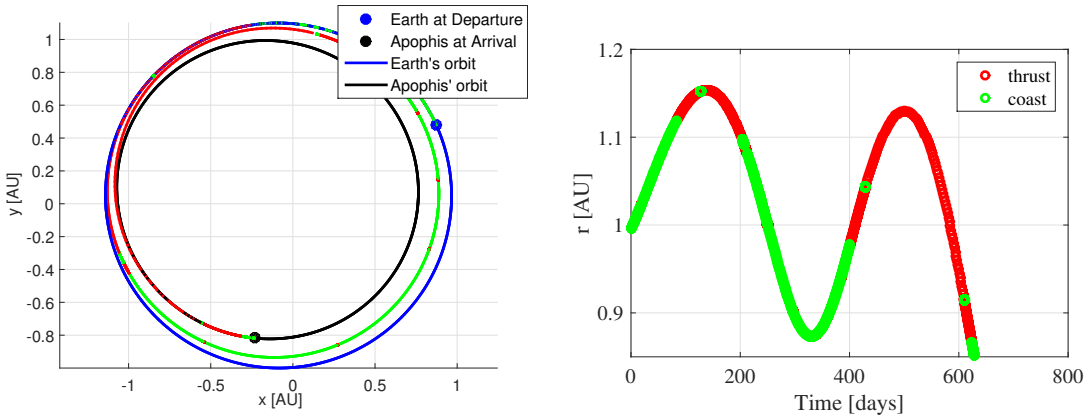

Figure 6: Nominal trajectory without any uncertainty (left) and corresponding spacecraft's distance from the Sun (right). Coast arcs are in green, thrust arcs are in red.

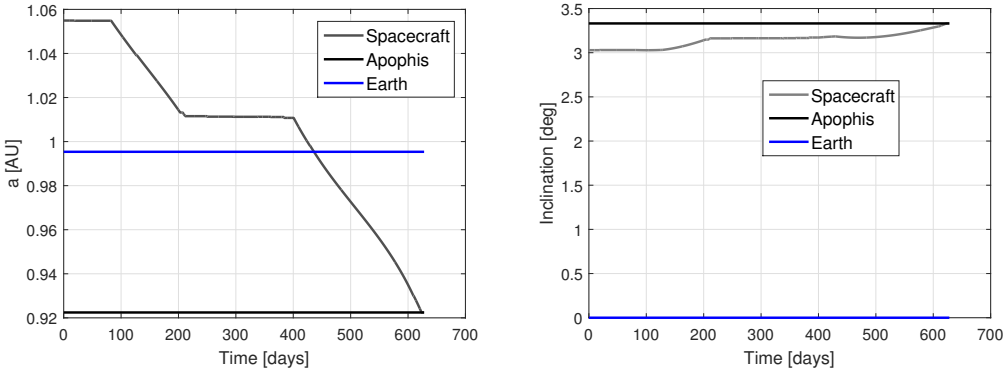

Figure 7: Variation of semi-major axis (left) and inclination (right) during the nominal transfer.

where also the value of the propellant mass has been relaxed with respect to the nominal value. In Problem (36), the aim is to maximise the Belief that the propellant mass is below or equal to 47 kg, while satisfying constraints relative to the targeted position and velocity. In particular, the Belief that $\Delta r \leq 3.2\ 10^6$ km and the Belief that $\Delta v \leq 0.91\ 10^6$ km/s should be higher than 0.95. The problem in Equation (36), is then expressed, using the function S, as:

$$\begin{aligned} &\max_{\boldsymbol{\xi}\in\Xi} \tilde{S}\left(\tilde{m}_{prop} \leq 47 \text{ kg}\right) \\ &\text{s.t.} \quad \tilde{S}(\widetilde{\Delta r} \leq 3.2\ 10^6 \text{ km}) > 0.965 \\ &\qquad \tilde{S}(\widetilde{\Delta v} \leq 0.91 \text{ km/s}) > 0.975\ . \end{aligned} \tag{37}$$

The values $\epsilon_{\Delta r,S} = 0.965$ and $\epsilon_{\Delta v,S} = 0.975$ of Problem (37) are obtained from $\epsilon_{\Delta r} = 0.95$ and $\epsilon_{\Delta v} = 0.95$ of Problem (36), using the iterative process described previously in the paper. The iteration starts from $\epsilon^0_{\Delta r,S} = \epsilon_{\Delta r}$ and $\epsilon^0_{\Delta v,S} = \epsilon_{\Delta v}$ and proceeds until correct values of $\epsilon_{\Delta r,S}$ and $\epsilon_{\Delta v,S}$ are located. The solution of Problem (37) is found using the method described in the previous sections and summarised in Figures 4 and 5; the results are presented in the following.

Uncertain Parameters Intervals and BPA The considered focal elements and their corresponding BPA are defined in Table 3. The number of considered focal elements is 48.

Internal Surrogate Models The number of training points $\mathcal{T}$ used to generate the internal surrogate models is $N_p = 1000$. The training points are generated on the focal elements in the space defined by $\boldsymbol{\xi}^L$ and $\boldsymbol{\xi}^U$ using

Table 3: Uncertain parameters intervals and associated BPA.

	v_∞ [km/s]			I_{sp,L_0} [s]		I_{sp,L_f} [s]		F_{L_0} [N]		F_{L_f} [N]	
Lower	3	3.2	3.55	2772	3010	2772	3010	0.0477	0.052	0.0477	0.056
Upper	3.1	3.5	3.7	2900	3388	2900	3388	0.05	0.0583	0.055	0.0583
BPA	0.2	0.5	0.3	0.4	0.6	0.4	0.6	0.2	0.8	0.3	0.7

a Halton sequence. DACE is used with a regression model with polynomial of order 2 and an exponential correlation model. 200 test points are used to validate the surrogate models. Table 4 shows the correlation coefficients $R\left(m_{prop}, \tilde{m}_{prop}\right)$, $R\left(\Delta r, \widetilde{\Delta r}\right)$ and $R\left(\Delta v, \widetilde{\Delta v}\right)$, for the 200 test points, considering models generated with different numbers N_p of training points. Data in Table 4 show that 1000 training points generate an accurate surrogate model. Figures 8 show the relationship between m_{prop} and $\tilde{m}_{prop}$, Δr and

Table 4: Correlation coefficients between real functions and surrogate models for different number of training points.

N_p	$R\left(m_{prop}, \tilde{m}_{prop}\right)$	$R\left(\Delta r, \widetilde{\Delta r}\right)$	$R\left(\Delta v, \widetilde{\Delta v}\right)$
50	0.9999	0.9958	0.99
200	0.9999	0.9992	0.9987
400	0.9999	0.9996	0.9993
1000	0.9999	0.9998	0.9995

$\widetilde{\Delta r}$, Δv and $\widetilde{\Delta v}$ for the 200 test points. As an example, the surfaces of the surrogate models for $\tilde{m}_{prop}$, $\widetilde{\Delta r}$ and $\widetilde{\Delta v}$, for a given uncertain vector $\boldsymbol{\xi}$, are shown in Figure 9, for different values of v_∞ and F_{L_0}, on the x and y axis, and for fixed values of the other uncertain parameters.

External Surrogate Models The external surrogate models are created using 150 training points generated by Halton sequence, using DACE with polynomial of order 2 and gaussian correlation model. Figure 10 shows the external surrogate models of S at the end of the iteration process described in Figure 4, for different values of v_∞ and I_{sp,L_0} (on the x and y axis) and for fixed values of the other uncertain parameters.

Results Figure 11 shows the curves of Bel and S corresponding to the 150 training points used to generate the external surrogate models. Each curve represented in Figure 11 corresponds, therefore, to a different vector of uncertain parameters, defined in the space Ξ, and to its corresponding feasible and optimal control. The figures also represent, by means of red vertical lines, the considered values of $\bar{\nu}_{m_{prop}}$, $\bar{\nu}_{\Delta r}$ and $\bar{\nu}_{\Delta v}$ for Problems (36) and (37). The red horizontal lines represent the chosen values of $1-\epsilon_{\Delta r}$, $1-\epsilon_{\Delta v}$, $1-\epsilon_{\Delta r,S}$ and $1-\epsilon_{\Delta v,S}$. Feasible solutions to Problems (36) and (37) are given by the uncertain vectors and corresponding controls that, for the values of $\bar{\nu}_{\Delta r}$ and $\bar{\nu}_{\Delta v}$ identified by the red vertical lines, provide a Bel or S curve that is above the red horizontal lines. Figures 12 show the Bel curves of the solutions of the iterative optimisation process described in Figure 4 to solve Problem 36. The maximum number of allowed iterations is 40. In order to make the final results easier to visualise, Figures 13 show the Bel curves for the controls corresponding to three uncertain vectors:

- the nominal uncertain vector $\boldsymbol{\xi}_{nom}$ (Table 2), represented in blue in Figure 13;
- the uncertain vector corresponding to the robust solution of Problem 36, identified by $\boldsymbol{\xi}_{rob}$, and represented in black in Figure 13;
- an additional solution found during the iterative process described in Figure 4, which does not satisfy the constraints defined in Problem 36. This solution is identified as $\boldsymbol{\xi}_{non-rob}$ and it is shown in green in Figure 13.

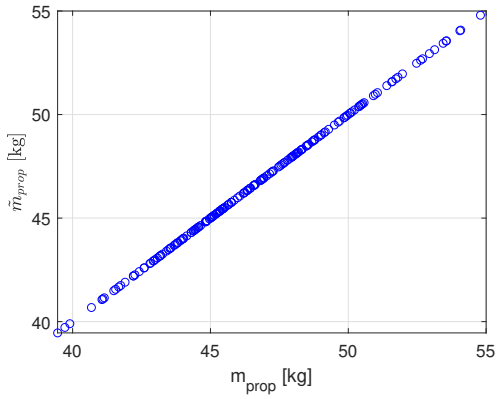

(a) Accuracy of $\tilde{m}_{prop}$.

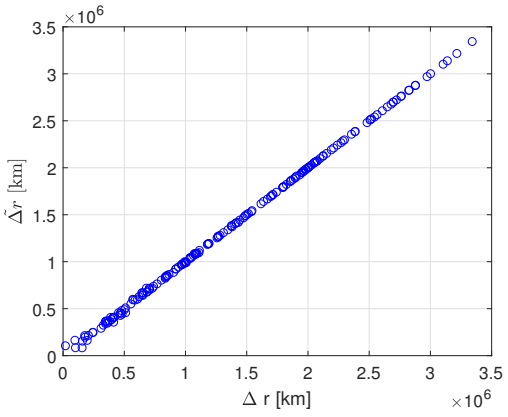

(b) Accuracy of $\widetilde{\Delta r}$.

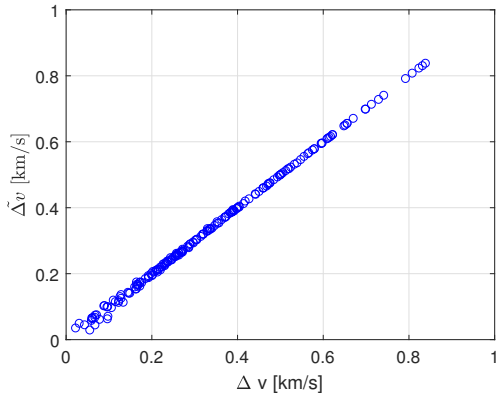

(c) Accuracy of $\widetilde{\Delta v}$.

Figure 8: Relationship between m_{prop} and $\tilde{m}_{prop}$ (a), Δr and $\widetilde{\Delta r}$ (b), and Δv and $\widetilde{\Delta v}$ (c).

Figure 13.a shows that the nominal solution has a Belief of the objective, for the chosen value of $\nu_{m_{prop}}$, equal to 0.12. In order to get a Belief equal to 1 using the nominal control, the mass of propellant has to be increased to 55.5 kg. The Belief of the constraints for the nominal solution are both equal to 1, for the chosen values of $\nu_{\Delta r}$ and $\nu_{\Delta v}$. The robust solution $\boldsymbol{\xi}_{rob}$, identified solving Problem 36, has a value of $Bel(m_{prop} \leq \bar{\nu}_{m_{prop}})$ higher than the one of the nominal solution, equal to 0.74. Moreover, when considering the robust solution, the Belief of the propellant mass reaches 1 when the mass of propellant is equal to 49 kg. The improvement in the Belief of the objective comes with a small reduction in the values of $Bel(\widetilde{\Delta r} \leq \bar{\nu}_{\Delta r})$ and $Bel(\widetilde{\Delta v} \leq \bar{\nu}_{\Delta v})$, which are, however, still above the chosen values of 0.95. Finally, the solution $\boldsymbol{\xi}_{non-rob}$, represented in green, shows that the method presented in Figure 4 is capable of locating many different solutions, characterised by different values of the Belief for the objective and the constraints. The Belief of the propellant mass corresponding to $\boldsymbol{\xi}_{non-rob}$, which is equal to 1, is, in fact, higher than the corresponding Belief of $\boldsymbol{\xi}_{rob}$ and $\boldsymbol{\xi}_{nom}$. However, this comes with a reduction of $Bel(\widetilde{\Delta v} \leq \bar{\nu}_{\Delta v})$ to a value smaller than 0.95.

During the iterations, the error due to the use of the external surrogate models is evaluated at each iteration, after the values of S for each $\boldsymbol{\xi}_{opt}$ are evaluated according to the method described in Figure 5. It is found

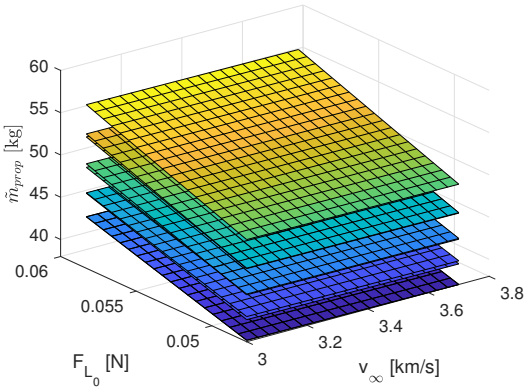

(a) Internal surrogate model $\tilde{m}_{prop}$.

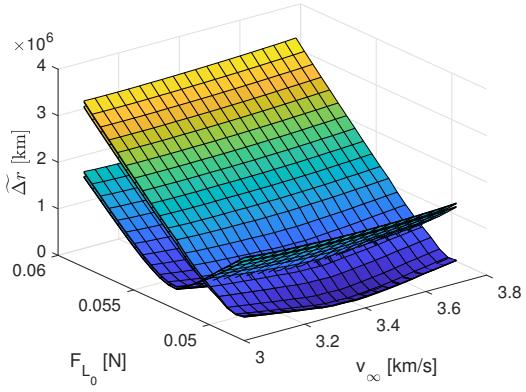

(b) Internal surrogate model $\widetilde{\Delta r}$.

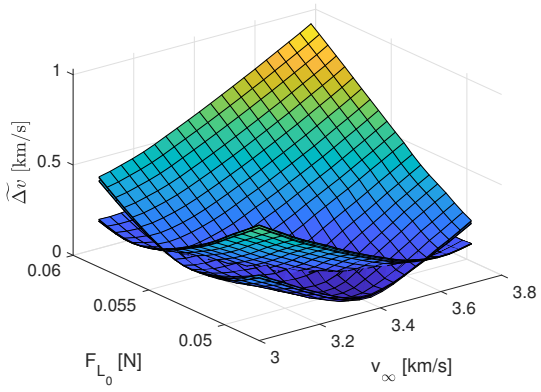

(c) Internal surrogate model $\widetilde{\Delta v}$.

Figure 9: Example of internal surrogate models $\tilde{m}_{prop}$ (a), $\widetilde{\Delta r}$ (b), and $\widetilde{\Delta v}$ (c), for different values of F_{L_0} and v_∞ (x and y axis), and for fixed values of the other uncertain parameters.

that, during the 40 iterations, the errors are:

$$\begin{aligned}
&|\tilde{S}\left(\tilde{m}_{prop} \leq \bar{\nu}_{m_{prop}}\right) - S\left(\tilde{m}_{prop} \leq \bar{\nu}_{m_{prop}}\right)| < 0.15 \\
&|\tilde{S}\left(\widetilde{\Delta r} \leq \bar{\nu}_{\Delta r}\right) - S\left(\widetilde{\Delta r} \leq \bar{\nu}_{\Delta r}\right)| < 0.03 \\
&|\tilde{S}\left(\widetilde{\Delta v} \leq \bar{\nu}_{\Delta v}\right) - S\left(\widetilde{\Delta v} \leq \bar{\nu}_{\Delta v}\right)| < 0.015
\end{aligned} \tag{38}$$

The errors are, therefore, limited to small values, and they are considered acceptable. It is important to stress that the aim of the proposed method is to obtain a surrogate model that is locally accurate in the region where the solutions of the considered problem are located; therefore, the surrogate models does not have to be globally accurate in the entire design space. Figure 14 shows the control solution, in terms of azimuth and elevation angles during the transfer, for $\boldsymbol{\xi}_{nom}$ and $\boldsymbol{\xi}_{rob}$. The difference in the control shown in Figure 14 produces the difference in the Belief curves seen in Figure 13.

Computational Times In the following, the computational times required to complete each block in Figures 4 and 5 are given. The computational times refer to a code run on Matlab R2017b on a machine with Intel(R) Core(TM) i7-3770 CPU @3.40 GHz and 8 GB RAM. In particular, with reference to Figure 5:

- The solution of the NLP problem takes ≈ 40 sec;

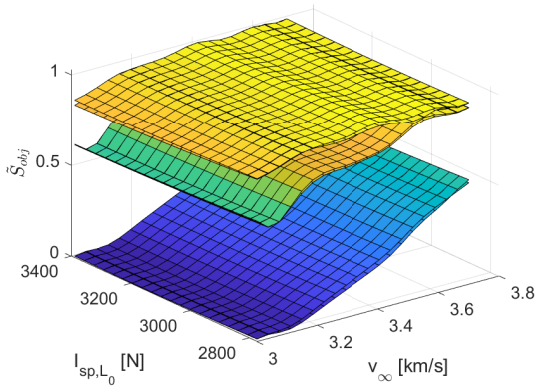

(a) External surrogate model $\tilde{S}_{m_{prop}}$.

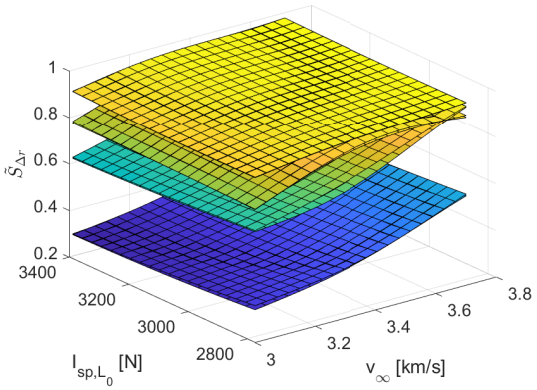

(b) External surrogate model $\tilde{S}_{\Delta r}$.

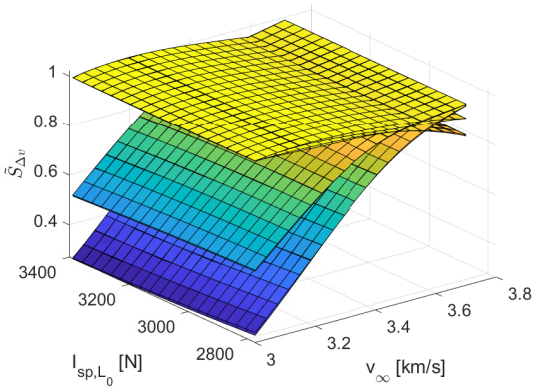

(c) External surrogate model $\tilde{S}_{\Delta v}$.

Figure 10: External surrogate model $\tilde{S}_{obj}$ (a), $\tilde{S}_{\Delta r}$ (b), and $\tilde{S}_{\Delta v}$ (c).

- The creation of the internal surrogate models takes ≈ 40 sec;
- The computation of the Bel takes approximately 3 minutes, while the computation of the function S takes 8 seconds. The difference in these computational times is due to the fact that the computation of the Belief requires a maximisation over each one of the 48 focal elements, for each one of the three functions $\tilde{m}_{prop}$, $\widetilde{\Delta r}$ and $\widetilde{\Delta v}$. The computation of the function S requires, instead, only the evaluation of these functions at a given number of points.

With reference to Figure 4:

- The computation time required for the computation of Bel and S, for all the N training points in Ξ, is given by the multiplication of N by the total computational time required to complete the diagram flow in Figure 5 (4 minutes and 30 seconds, approximately). In this case, $N = 150$ and the total computational time to evaluate all the training points is, therefore, approximately 11.25 hours;
- The time required to create the external surrogate models for S, using the training points and DACE, is ≈ 0.5 seconds;
- The time required to solve Problem (37), when 10000 function evaluations are considered for MP-AIDEA, is 10 seconds. As a comparison, if surrogate models of S were not used, and the complete

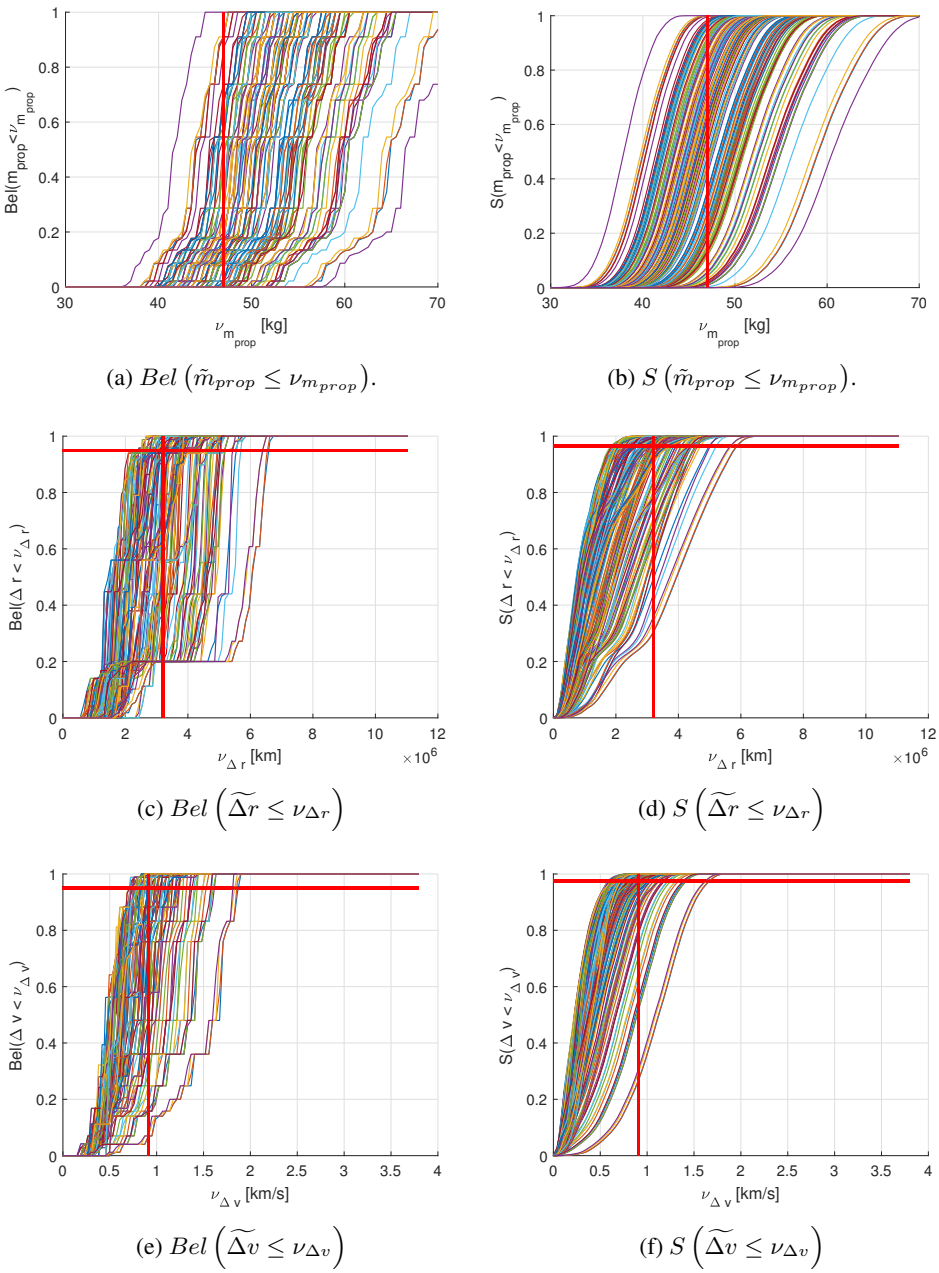

(a) $Bel\left(\tilde{m}_{prop} \leq \nu_{m_{prop}}\right)$. (b) $S\left(\tilde{m}_{prop} \leq \nu_{m_{prop}}\right)$.

(c) $Bel\left(\widetilde{\Delta r} \leq \nu_{\Delta r}\right)$ (d) $S\left(\widetilde{\Delta r} \leq \nu_{\Delta r}\right)$

(e) $Bel\left(\widetilde{\Delta v} \leq \nu_{\Delta v}\right)$ (f) $S\left(\widetilde{\Delta v} \leq \nu_{\Delta v}\right)$

Figure 11: Bel and S curves of the training points, corresponding to the objective (a and b), position constraint (c and d), and velocity constraint (e and f).

process described in Figure 5 were to be realised, instead, at each function evaluation of the optimiser, the total computational time would have been 10000×4.5 min ≈ 750 hours;

- The computation time to compute Bel and S for $\boldsymbol{\xi}_{opt}$ is equal to the time required to complete the steps in Figure 5, that is, approximately 4 minutes and 30 seconds;

- The time required to update the surrogate models for S is approximately 0.5 seconds.

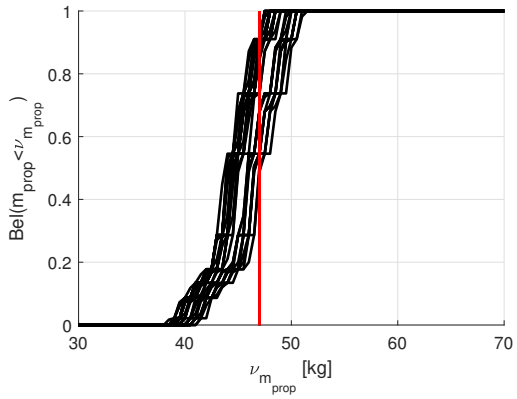

(a) $Bel\left(\tilde{m}_{prop} \leq \nu_{m_{prop}}\right)$.

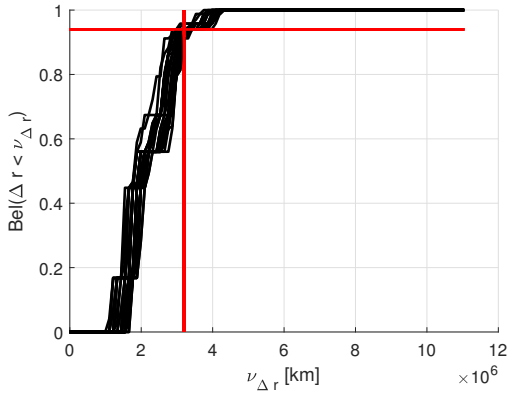

(b) $Bel\left(\widetilde{\Delta r} \leq \nu_{\Delta r}\right)$

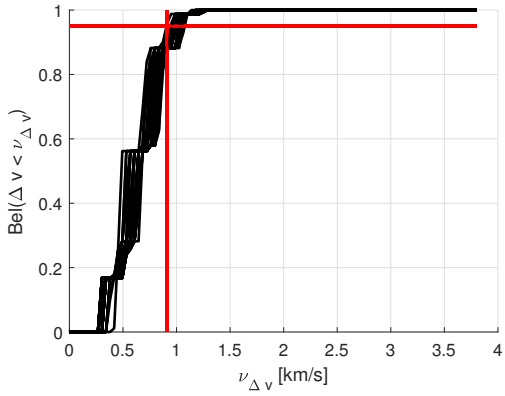

(c) $Bel\left(\widetilde{\Delta v} \leq \nu_{\Delta v}\right)$

Figure 12: Bel and S curves of the results of the optimisation problem, corresponding to the objective (a), position constraint (b), and velocity constraint (c).

CONCLUSION

This paper has presented the formulation and solution of the optimal control problem under uncertainty, where the uncertainty has been modelled using the Belief function of the Evidence Theory. In this work, the computation of the Belief function, which requires an optimisation over each focal element of the uncertainty space, has been sped up using internal surrogate models of the quantities to optimise. The original exact formulation of the problem, that uses the discontinuous Belief function, has then been transformed into an inexact formulation using a new continuous statistic function, S. The optimisation has then been realised on the surrogate of the function S, rather than on the Belief. Moreover, by exploiting the correspondence between space of uncertainties and space of feasible and optimal controls, the optimisation has been realised on the space of uncertainties, rather than on the higher dimensional space of the controls. The method has been applied to the low-thrust transfer from Earth to asteroid Apophis. The considered uncertain parameters are the magnitude of the hyperbolic excess velocity at launch, and four parameters describing the thrust and specific impulse of the low-thrust engine and their variation during the transfer.

The use of surrogate models and the optimisation on the uncertainty space, rather than on the space of the controls, have solved some of the challenge associated to the original formulation of the problem of optimisation under uncertainty, transforming the original problem into a manageable one, that can be solved in a limited computational time. Moreover, results have shown that the proposed method is able to locate the

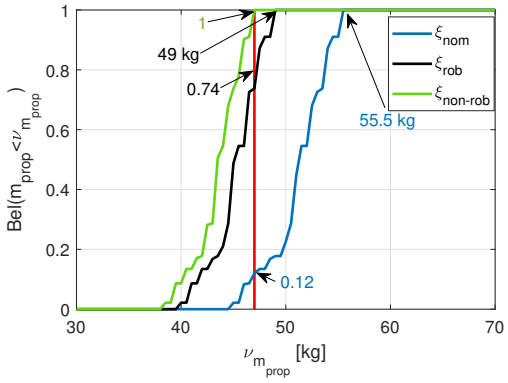

(a) $Bel\left(\tilde{m}_{prop} \leq \nu_{m_{prop}}\right)$.

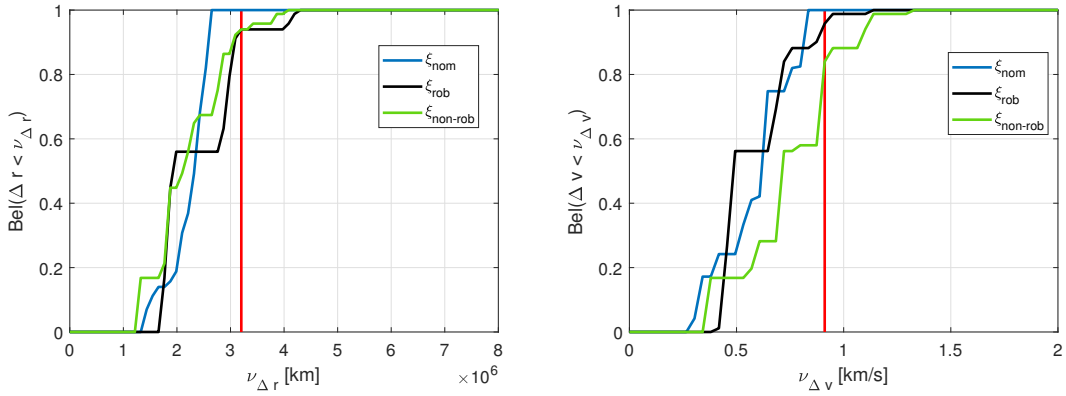

(b) $Bel\left(\widetilde{\Delta r} \leq \nu_{\Delta r}\right)$ (c) $Bel\left(\widetilde{\Delta v} \leq \nu_{\Delta v}\right)$

Figure 13: Belief of the nominal solution ($\boldsymbol{\xi}_{nom}$), of the robust solution ($\boldsymbol{\xi}_{rob}$), and of a non-robust solution ($\boldsymbol{\xi}_{non-rob}$).

control vector that provides a solution that is robust to uncertainties.

In this work, the proposed method has been applied to a problem with five uncertain parameters. The method could also be applied to higher dimensional problems. For higher dimensional problems, an increased computational time has to be expected. The increase in computational time is due to the increase in the number of focal elements over which to realise the maximisation for the computation of the Belief of the training points of the external surrogate models. In addition, an increased number of training points would likely be required to obtain sufficiently accurate initial external surrogate models.

Future work will be devoted to transform the constrained single-objective optimisation problem into a multi-objective optimisation problem, where the variables $\nu_{m_{prop}}$, $\nu_{\Delta r}$, $\nu_{\Delta v}$, $\epsilon_{\Delta r}$ and $\epsilon_{\Delta v}$ are also minimised. Moreover, the proposed method will be modified in order to extend the search for the robust solution to the space of all the admissible controls, so as to include also the non-feasible and non-optimal controls.

ACKNOWLEDGEMENTS

This research has been developed with the partial support of the CNES grant R-S17/BS-0005-034 ”Robust Optimization of Low-Thrust Interplanetary Trajectories” and the H2020 MCSA ITN UTOPIAE grant agreement number 722734.

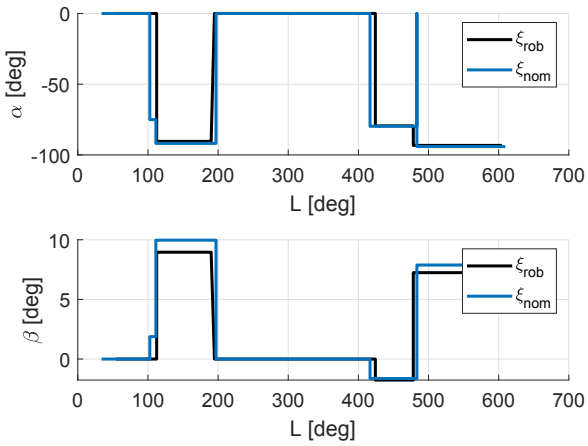

Figure 14: Controls (azimuth and elevation angles α and β during the transfer) corresponding to $\boldsymbol{\xi}_{nom}$ and $\boldsymbol{\xi}_{rob}$.

REFERENCES

[1] M. Vasile, "Robust Mission Design Through Evidence Theory and Multiagent Collaborative Search," *Annals of the New York Academy of Sciences*, Vol. 1065, 2005, pp. 152–173.

[2] N. Croisard, M. Vasile, S. Kemble, and G. Radice, "Preliminary space mission design under uncertainty," *Acta Astronautica*, Vol. 66, 2010, pp. 654–664.

[3] G. Shafer, *A Mathematical Theory of Evidence*. Princeton University Press, 1976.

[4] M. Vasile, E. Minisci, and Q. Wijnards, "Approximated Computation of Belief Functions for Robust Design Optimization," *53rd AIAA/ASME/ASCE/AHS/ASC Structures, Structural Dynamics and Materials Conference, Honolulu, Hawaii, 2012*, 2012.

[5] A. P. Dempster, "Upper and Lower Probabilities Induced by a Multivalued Mapping," *The Annals of Mathematical Statistics*, Vol. 38, No. 2, April 1967, pp. 325–339.

[6] L. Zhang, "Representation, independence, and combination of evidence in the Dempster-Shafer theory," *Advances in the Dempster-Shafer theory of evidence* (R. R. Yager, J. Kacpryk, and M. Fedrizzi, eds.), ch. 3, pp. 51–69, New York: John Wiley and Sons, 1994.

[7] K. Sentz and S. Ferson, "Combination of Evidence in Dempster-Shafer Theory," tech. rep., Sandia National Laboratories, 2002.

[8] M. Di Carlo, M. Vasile, and E. Minisci, "Multi-population inflationary differential evolution algorithm with adaptive local restart," *2015 IEEE Congress on Evolutionary Computation (CEC)*, 2015, pp. 632–639.

[9] F. Zuiani, M. Vasile, A. Palmas, and G. Avanzini, "Direct transcription of low-thrust trajectories with finite trajectory elements," *Acta Astronautica*, Vol. 72, 2012, pp. 108–120.

[10] M. Di Carlo, J. M. Romero Martin, and M. Vasile, "CAMELOT - Computational Analytical Multi-fidElity Low-thrust Optimisation Toolbox," *CEAS Space Journal*, 2017.

[11] F. Zuiani and M. Vasile, "Extended analytical formulas for the perturbed Keplerian motion under a constant control acceleration," *Celestial Mechanics and Dynamical Astronomy*, Vol. 121, No. 3, 2015, pp. 275–300.

[12] S. N. Lophaven, H. B. Nielsen, and J. Sondergaard, "DACE - A Matlab Kriging Toolbox," tech. rep., Technical University of Denmark, 2002.